Heliyon 10 (2024) e33384

Contents lists available at ScienceDirect

Heliyon

journal homepage: www.cell.com/heliyon

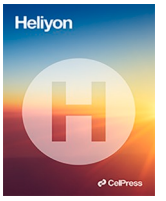

Research article

Airflow detailed analysis through a face mask using the schlieren technique

Cornelio Alvarez-Herrera [a], Jose G. Murillo-Ramirez [a,b,*]

[a] Facultad de Ingeniería, Universidad Autónoma de Chihuahua, Nuevo Campus Universitario, Circuito, Universitario S/N, 31125, Chihuahua, Chih., Mexico
[b] Centro de Investigación en Materiales Avanzados S. C., Miguel de Cervantes 120, 31136, Chihuahua, Chih., Mexico

ARTICLE INFO

Keywords:
Airflow through a face mask
Schlieren optical arrangement
Airflow particles velocity

ABSTRACT

This work presents an exhaustive visualization of the airflow expulsed by a person while breathing, talking, exhaling, and blowing inside a closed room wearing a disposable face mask like those used in hospitals for patient protection and those who care for them. An optical schlieren experimental arrangement was used to obtain some of the relevant physical characteristics of the airflow, such as its refractive index gradient, the distribution of temperature, and the associated velocity field for all the tests developed. We tested three face masks, one of the surgical types and the others of the N95 series with denominations KN95 and 3MN95 (Aura TC-84A-8590). The results show appreciable differences between the masks evaluated; the surgical mask was the one that allowed the most abrupt output airflow through it in the field of view of the experimental setup. However, were also found some differences in the performance of the KN95 and 3MN95 masks. The KN95 face mask had the best performance since it expulsed to its surroundings the lowest airflow with different physical properties to the input airflow. The results obtained are relevant since it was possible to estimate the expulsed airflow velocity as a function of the distance for every face mask tested, which allows for understanding its filtering capacity by restricting the flow of potential pathogens from the mouth or nose of one person to another. Undoubtedly, the airflow behavior determination around a face mask can help to reduce the risk of spreading infectious airborne particles.

1. Introduction

The security of people while breathing within indoor environments such as buildings, hospitals, workplaces, and classrooms, only to mention some public sites, is a pressing need. The productivity and job performance, including all other daily activities, of people depend on their health. For this reason, it is necessary to ensure both the security and the commodities required to stay in public environments. In particular, verifying the quality of air that breaths every one of us in these collective sites has a high priority and constitutes a research field of high importance that is necessary to aboard immediately. Recent acute health problems worldwide among people associated with respiratory diseases such as severe acute respiratory syndrome coronavirus 2 (SARS-CoV-2) that causes COVID-19 have highlighted the need for accelerating research on this subject. The application of new methodologies to detect and quantify the air quality in public environments in real time is every day more necessary to guarantee the security of all of us.

* Corresponding author. Centro de Investigación en Materiales Avanzados S. C., Miguel de Cervantes 120, 31136, Chihuahua, Chih., México.
E-mail address: jose.murillo@cimav.edu.mx (J.G. Murillo-Ramirez).

https://doi.org/10.1016/j.heliyon.2024.e33384
Received 3 November 2023; Received in revised form 20 June 2024; Accepted 20 June 2024
Available online 21 June 2024

Since some years ago, it has been determined that many respiratory diseases in humans spread through airborne mechanism, whether in the form of saliva droplets, saliva nuclei, or powder [1]. However, there are other transmission mechanism, including direct contact with sick people or animals or indirect contact through their secretions, infected body fluids, or touching contaminated objects. As is known, upper respiratory tract infections involve self-limited inflammation of the upper airways with associated cough, but without signs of pneumonia in patients with no other affectation that can explain their symptoms [2,3]. Two fundamental properties of aerosols determine the seal level of the personal protective equipment (PPE) around the airways: a) their tendency to follow airflows and b) their small size, in the case of bioaerosols, which demands a higher filtering capacity [4]. For purposes of human health risk during the breathing process two types of particles are usually important to consider; a) inhalable, and b) respirable particles. Inhalable particles refer to coarse particles that can be breathed into the nose or mouth with an aerodynamic diameter >2.5 μm, often defined as the fraction between 2.5 and 10 μm [5–7]. Nevertheless, some authors classify the inhalable particles as those with sizes ≤ 100 μm [5,6,8]. While the respirable particles, often defined as fine particles with an aerodynamic diameter of <2.5 μm, are a sub-set of inhalable particles, covering any "fraction of inhaled airborne particles that can penetrate beyond the terminal bronchioles into the gas-exchange region of the lungs [5–7].

On the other hand, the transmission of infectious particles from one individual to another is possible through the production of infectious droplets, which are projected when breathing, speaking, coughing, or sneezing [4,9]. Transport of these pathogen-laden droplets in the environment is critically important in the transmission of respiratory infectious diseases. Long-range aerosol transmission occurs when small enough droplets of infectious material remain airborne almost indefinitely and be transmitted over long distances [10,11]. The viability of an infectious agent can be affected by many environmental factors, including temperature, humidity, and airflows that can lead to dehydration. The size of droplets or bioaerosols released from a person talking, sneezing, or coughing and the airflow patterns that carry them determine how they move. The relative humidity of the environment alters the evaporation rate of these droplets and, thus, their size. On the other hand, droplets in dry air evaporate quickly, shrinking their size and falling to the ground more slowly, being able to stay suspended in the air longer [4,11]. It is relevant to take it into account since the transmission from the respiratory tract of one person to another is possible if the density of pathogen organisms in such droplets is not negligible and remains for a sufficient time airborne to be inhaled. In summary, the upper respiratory tract infections are caused by airborne particles containing bacteria, spores or viruses such as influenza and SARS-CoV-2 only to mention some of them. Unfortunately, these diseases are here to stay, and people worldwide will continue to get sick of them. Therefore, the study of airflow dynamics that can be inhaled or breathed by a person whether wearing a face mask or even without one is and will be a current research subject for many more years, which justifies the relevance of a study as we present in this work.

There are some reports in the literature about the efficiency of some of the face masks that people currently use, which certainly have contributed to understanding the transmission mechanisms of infectious particles via airborne [12–15]. However, there is still a need to understand and develop robust and easy-to-apply methodologies to understand the dynamics of airflows expelled or inhaled by people wearing a disposable face mask or without it in a closed area to take precautions and avoid possible airborne infections. Thus, it is also relevant to evaluate the efficiency of some of the face masks used by people since some do not provide the necessary safety, and usually, it is unknown. Consequently, the present research is relevant since it gives elements to understand the dynamics of these inhaled or exhaled airflows, and indirectly, it evaluates in a certain way the filtering capacity of three of the representative face masks used nowadays.

In this research, we have developed a study to visualize the airflow expulsed or inhaled by a person while breathing, talking, exhaling, and blowing while wearing a disposable face mask inside a closed room. We are using the term "exhalation" as the flow of air that leaves an organism by expulsion from its lungs with certain efforts in the case of a human and later enters by aspiration or inhalation, which is the act of breathing air into the lungs. Breathing refers to the action of taking air into the lungs and sending it out less abruptly than in the case of exhalation and inhalation. The act of "blowing" consists of creating and sending out a stream of air from the mouth of the test subject. A person blows when he closes the lips of his mouth and resembles a funnel, as shown in Fig. 4 (test D).

It was examined the airflow behavior around a set of three face masks commonly used in the world by the non-invasive schlieren optical technique. The main objective of this research was to obtain some of the most relevant physical parameters of the airflow through the tested disposable face masks, such as the temperature in its surroundings, the velocity fields and an estimation of the expulsed airflow velocity as a function of the distance. Nevertheless, we hope to contribute to a safety qualitative evaluation of the face masks examined against the spread of particles from the user.

2. Theoretical background and respirator masks characteristics

2.1. Composition and effectiveness of face masks tested

The selection and use of PPE, such as respirators and eye protection, is highly relevant since it is activity-and environment-dependent [12,16,17]. Concerning about the respirators, the best respirator masks can filter particles as small as 0.007 μm, virus as the coronavirus with a size between 0.003 μm and 0.1 μm, bacillus bacteria with sizes between 0.25 μm and 20 μm, larger particles such as those with a characteristic diameter of 2.5 μm called PM2.5, red blood cell of 7 μm size, and dust particles of 10 μm (PM10) among other type of particles [5,6,13]. However, it is important to comment that the contagion of a disease by a person via some airborne virus depends on the size of the particles that carry it. Exhaled droplet size due to talking and coughing can be around 50–100 μm, although smaller droplets with a particle size of 10 μm or even 0.7 μm have also been detected [18,19]. Some respirator masks do not filter particles as small but can filter others with an average size of around some microns.

The present visualization study of the airflow expulsed by a person while breathing, talking, exhaling (breathe forth), and blowing inside a closed room was completed by examining three disposable face masks as those widely used around the world. One of these masks is of the surgical class, and the other two are of the N95 series: KN95, and 3MN95 (3 M Aura TC-84A-8590). The surgical mask usually has three-ply (three layers) of filters [20], and has a typical effectiveness ≥80 % when filtering particles with an average diameter of 3.0 μm as stipulated for example the China standard YY/T0969, while the N95 and the FFP2 series can have five or six layers of filters. The N95 and KN95 denominations are equivalent, although they have different certifications; series N95 follows the NIOSH (National Institute for Occupational Safety and Health) standard from the United States (U.S.) [21], and the KN95 complies with the GB2626 China standard [22]. N95s, usually cup-shaped, have two straps to secure around the head and a wire-nose bridge to fit tightly on the face and form a tight seal around the nose and mouth. It has been demonstrated that N95s respirators, whose effectiveness is 95 %, can filter large and small particles protecting the user from inhaling particles of SARS-COV-2, the virus that causes COVID-19. Of course, if the mask is fitted properly and all airflow goes through the filters rather than leaking around the sides. Recent studies have found that N95 respirators comply with the particles filtration efficiency standard (PFE), capturing and filtering particles as small as 0.1 μm in diameter, while the single-use face masks do not comply with this standard. N95 series has a filtration efficiency greater than or equal to 95 % against certain types of non-oily particles such as: pollen, cement, heavy metal, bacteria, soot, virus, asbestos, and mould, among other type of particles. In theory, the N95 and KN95 masks have the same filtering effectiveness (of particles difficult to capture, with an average diameter of 0.3 μm representing the most-penetrating particle size) ≥ 95 %. Europe follows the EN 149:2001 standard with three levels (FFP1, FFP2, and FFP3) of filtering effectiveness (under the same criteria of N95s series regarding particle capture) [23]. The FFP1 (Filtering Face Piece level 1), FFP2, and FFP3 levels refer to the filtering effectiveness of ≥80 %, ≥94 %, and ≥99 %, respectively. Therefore, the N95, KN95, and EN 149 FFP2 certifications for face masks are similar regarding filtration effectiveness. Respirator masks are classified according to the class of filters used for their manufacture. There are three classes of filter series, denominated: N, R, and P, whose effectiveness is 95 %, 99 %, and 99.97 %, respectively [21]. However, the selection of N, R, or P filter series depends on the presence or absence of oil particles. If no oil particles are present in the work environment, anything of the N, R, and P series can be used, but if there are oil particles, such as lubricants, cutting fluids, glycerin, etc., should be used R or P series [21].

The face masks used in this work have some differences between them, and therefore they offer specific protection depending on the materials and assemblage used in their manufacture. Fig. 1 shows a photograph of the standard face mask 3MN95, KN95, and the surgical type used in this study. All the face masks available in the market are made from several filter materials or multiple layers of plastic polymer, usually polypropylene (PP). However, the exact composition of the materials used in the mask assemblage is seldom reported by the manufacturers. The details about the face masks to the final consumer are limited to specifying their filtering capacity. Despite this, there is information about the materials commonly used for face mask manufacturing. One of these materials is called "*spun-bond*", made of 100 % polypropylene, which is recyclable, waterproof, and dust resistant, and whose surface density varies between 10 and 150 g/m^2 "*Melt-blown*" fabric made of submicron PP filaments with excellent filtration properties including electrostatic adsorption also is used in the face mask assemblage. Most respirator masks also contain at least one layer of "*hot cotton*" fabric, a thermoplastic polymer made from PP, commonly used in medical devices, food packaging, films, plastic furniture, and automotive parts. To give an idea of the pores size and the morphology of each material employed in the fabrication of the face masks used in this study, a Hitachi SU3500 scanning electron microscope (SEM) was used. The morphology observation of the surface of each layer at high resolution required the deposition of a thin film of gold. Fig. 2 shows a series of SEM micrographs of representative zones in each one of the three layers composing the surgical-type face mask used, and a selected zone in each one of the five layers that constitute the KN95 and 3MN95 face masks used in this research. As shown in Fig. 2(a)-2(m) the size of pores in each layer varies depending on the examined material. In Fig. 2(k) and (m) can be observed for the three-ply surgical-type face mask pores with sizes greater than 100 μm for the outer and inner layers, while in the intermediate layer (Fig. 2(l)) they are smaller on the order of 60 μm. On the other hand, some layers of the KN95 and 3MN95 face masks can have pores with characteristic lengths equal to 15, 20, 30, 40, and 60 μm as shown in Fig. 2(a)-2(j). Hence, there is the need to use several layers of polypropylene so that its overlapping can reduce the size of these pores on average to smaller dimensions to prevent the passage of particles through the airflow in the face mask. Of course, some of these layers have the function of electrostatically trapping some of the particles before they pass through the next layer. It is known that

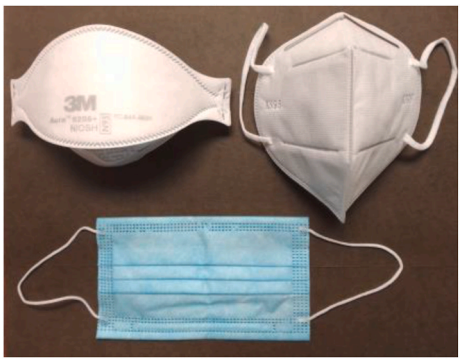

Fig. 1. Standard face mask 3MN95 (Aura TC-84A-8590) (left), KN95 (right) and surgical (down) used in this study.

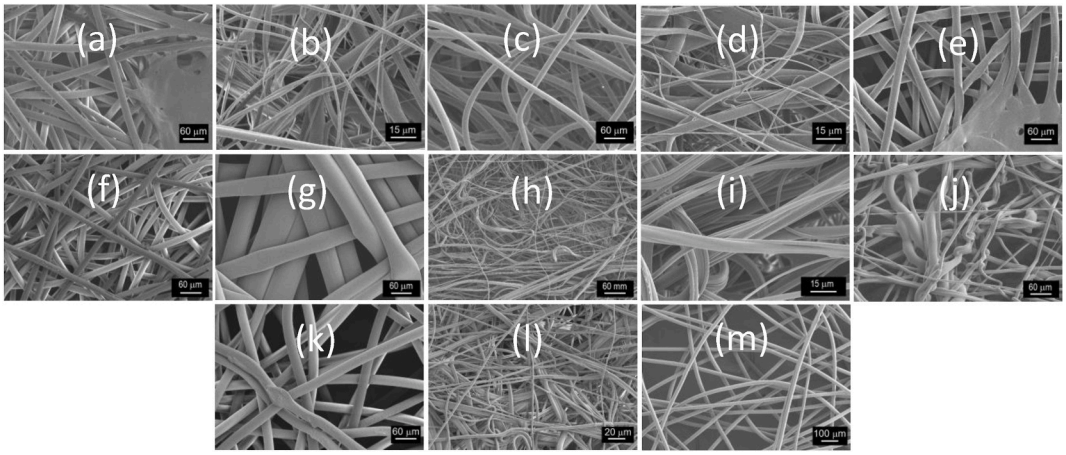

Fig. 2. SEM micrographs of representative zones of the five layers of PP constituting the KN95, 3M95, and the three layers of the surgical three-ply face masks used in this research. From outer to inner, layer (a), (b), (c), (d), and (e) (such that layers (e), (j), and (m) correspond to the inner surface that was in contact with the face of the subject performing the tests) correspond to KN95, and (f), (g), (h), (i) and (j) to 3MN95 face masks, respectively. Micrographs (a), (c) and (e), (f), (g), (h), and (j) were obtained at a magnification of 200×; (b), (d), and (i) at 1000×. (k), (l), and (m) are the selected zones of the layers of the surgical three-ply face mask, (k) and (l) were obtained at a magnification of 200×, and (m) at 100×.

particles larger than 0.3 μm are mainly captured by inertial impaction, whereas particles below 0.2 μm are retained by filtration and electrostatic attraction [24]. Fig. 2(k) shows how the outer and the inner Fig. 2(m) PP layers constituting the surgical-type face mask have a pore size larger than the average pore size of the PP layers in the KN95 (Fig. 2(a)-2(e)) and 3MN95 (Fig. 2(f)-2(j)) face masks. Also, as can be observed in Fig. 2(a)-2(j), there are some appreciable differences in the morphology of the inner layers of the KN95 and 3MN95 face masks. The inner layers of the 3MN95 face mask (Fig. 2(g)-2(j)) present PP fibers with more inhomogeneity, disorder, and pores greater than in the corresponding layers of the KN95 face mask, as shown in the micrographs 2(b)-2(e). These specific characteristics of the PP layers in both face masks determine their filtering efficiency.

2.2. Schlieren technique

The schlieren word comes from the German term “schliere” which means inhomogeneity and has given the name to the schlieren optical technique used for determining changes or inhomogeneities in the density of transparent samples of solids, liquids, or gases. Schlieren technique, due to suitable and easy implementation has been used in the study of the dynamics of transparent fluid flows, in the quality control of optical lenses employed in microscopes and telescopes, in the visualization of combustion gases of a flame used to determine the efficiency of the combustion process, and in the measurement of the velocity of waves propagating in fluids, only for mention some of their diverse applications [25–27].

One of the most attractive advantages of the schlieren optical technique is its no-intrusiveness, especially in the study of flows of gases and fluids. Essentially, the schlieren technique obtains relevant information about the object or media of interest from the images

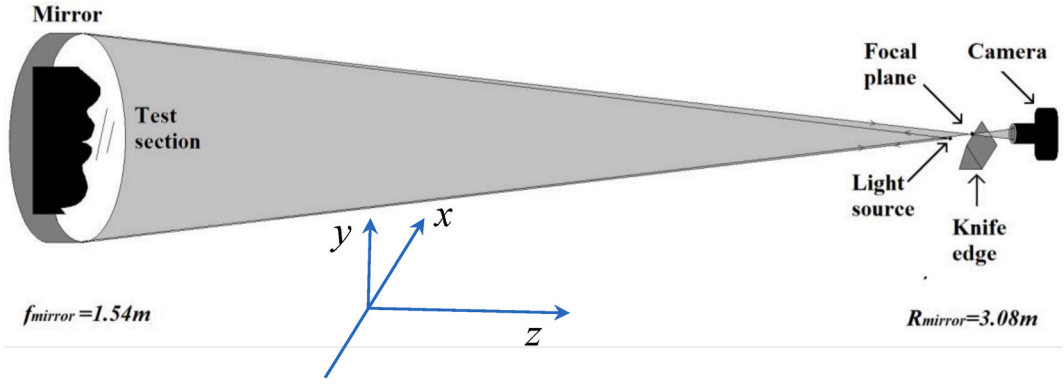

Fig. 3. Schematic diagram of the single mirror schlieren experimental set-up used in this research to visualize the airflow expulsed by a person while talking, breathing, exhaling, and blowing, wearing a disposable face mask. The spherical mirror has a diameter D = 0.15 m and a focal distance f = 1.54 m. The distance from the test section to the knife-edge mirror was 3.08 m. The light source used was a small white led placed behind of a metallic plate with a pinhole of 2 mm dimeter. The airflow examined was sent in the x direction, perpendicularly to the light beam path.

acquired once they have deviated a light beam from its original path [25,27]. For example, the inhomogeneities in the air density induced by a flame, dust, or other airborne particles and the non-uniformity in the composition of fluids and solids placed in the path of a light beam can refract it, and thus, deviate it from its original propagation direction. In the study case of gases, the schlieren technique quantifies the refractive index gradients in a projection plane caused for example by the hot gases distributed inside a volume, integrating the obtained information along an optical path [27]. Usually, the schlieren technique provides information in a projection plane, i.e., in two dimensions. Nevertheless, it is possible to estimate three-dimensional details of the volumetric object of interest either employing projections at different angles to reconstruct a volumetric object using the Radon transform or under the assumption of cylindrical geometry applying the Abel transform [27]. In this way, after processing and analyzing the images of the objects or media of interest obtained in real-time by a camera, it is possible to characterize either the streamline of an airplane model within a wind tunnel or determine at a specific point the temperature and velocity of a fluid flow, only for mention some application examples.

In this research we have used the schlieren technique to visualize the gradient of refractive index of the air in two-dimensions in a projection plane, caused by the breath of a person using a face mask who was placed in the path of a light beam propagating in a closed room. Fig. 3 shows a schematic representation of the physical principle that describe the single mirror schlieren optical technique. As shown in Fig. 3, an incident light ray traveling along the z direction and propagating through a test volume of air, which is the object of study, with a refractive index $n = n(x, y, z)$ undergoes an angle deflection and forms a projection of object in the image plane. A knife edge placed at the image plane helps make the system sensitive to changes in the refractive index that can be detected and recorded by the camera positioned at the end of the experimental setup. Also, it is possible to obtain the temperature fields of the air test volume from its density as described in Refs. [25,27]. Nevertheless, in this research were obtained the temperature fields indirectly from the fluid density fields at a reference temperature measured with a K-type thermocouple and a digital multimeter.

3. Experimental procedure

3.1. Schlieren experimental setup

The experiments of this research were carried out in a closed room with dimensions equal to 3 m wide x 6 m long x 4 m high, approximately 72 m^3 in size, maintaining shut its window and door at room temperature. The temperatures of the room and a zone in front of each face mask, close to the mouth (3 cm) of the person who completed all the tests (a 28-year-old female subject with a weight of 57 kg) were measured with a K-type thermocouple coupled to a 2110 KEITHLEY digital multimeter. The person who performed each of the tests was placed at a distance of 5 cm from the single mirror schlieren experimental setup, sitting on a chair and resting her head on a small table with lateral supports to avoid movements as much as possible while carrying out the speaking, breathing, exhaling, and blowing tests in this research. The small table where the test subject rested her head was placed on a holographic table in our laboratory. The airflow to be examined was sent perpendicularly to the light beam path, as shown in Fig. 3. The experimental schlieren setup used is very similar to that described in Ref. [14] that was employed to perform a similar study to the one presented in this research. In Ref. [28], a similar schlieren optical system was used to record speech airflow with 14 different face masks, comparing it to mask-less. That study has shown the benefit of using a face mask since its use restricts the airflow from a speaker. Nevertheless, we have carried out the investigations about the airflow through the face mask a step ahead of Refs. [14,28] since we have measured some physical parameters of the airflow not considered or calculated previously. Specifically, the exhaustive processing of the schlieren videos recorded allowed us to obtain 64 images with high contrast (without the noise of the optical system) of the refractive index gradient induced by the airflow in front of each face mask considered. Next, the temperature fields in a zone near the front of each respirator mask were calculated using the gradient of the refractive index of air previously obtained. Finally, the airflow speed that escapes from each face mask considered for each airflow test studied was estimated.

Our experimental setup is a double-pass off-axis schlieren system where the light beam from the source passes through the flow toward the test section. From that position, the mirror reflects the light beam and sends it through the flow again until it reaches the focal plane of the optical system. At the focal plane is found a knife edge, which makes the system sensitive to changes in the refractive index of air in the y direction. Therefore, the refractive index gradient of air was analyzed in the y direction. It is important to comment that the light beam passes twice through the flow (approximately twice the focal length of the spherical mirror ($2f_{mirror} = R_{mirror}$)), which makes the optical system doubly sensitive [29] and allows for increasing the angle at which the light rays are deflected.

In our procedure, first, a reference image of the incident light beam traveling along the schlieren experimental set-up at room temperature captured by a photographic camera was taken. Next, we continued with the visualization of the physical characteristics of the airflow expulsed by the person who completed all the tests. It was taken a short video with a duration of around 1 min of each one of the tests considered in this study shown in Appendix A. Supplementary material. Each one of videos were recorded with an 8-bit pixel depth in avi format using a CMOS digital camera, acquiring 45.05 frames per second at a full spatial resolution of 752 $\times$ 480 pixels. However, only a selected zone of interest of 211 $\times$ 97 pixels of the full picture was analyzed. A convergent lens with a diameter of 2.54 cm and a focal length of 50 cm was coupled to the CMOS digital camera to improve the capture of images constituting the video.

3.2. Processing images methods

The temperature distribution fields post processed from the schlieren images were calculated by obtaining first the refractive index gradient of air in the y-direction from a short video of each airflow test (acquired in avi format) considered in this work. A reference video of the zone around the face mask, without airflow, was also acquired. Both videos were edited with FFMPEG software to obtain

representative images in jpg format of a specific airflow test around the face mask and representative images of the reference without airflow. Next, an image without airflow was subtracted from a selected image with airflow to reduce the noise and imperfections of the optical system so that finally it is obtained a clean image with the airflow. The image without noise is the gradient field of the refractive index of air, which then is linearly integrated into the y-direction, taking into account each pixel column of the image to obtain the refractive index in two dimensions. Due to the refractive index n of air depending linearly on the airflow density ρ according to the Gladstone-Dale relation, $n\text{-}1 = k\rho$ [29] (where k is a constant dependent on the media properties and the experimental setup), it is possible to obtain the density field using the gradient field of the refractive index previously found. In the following step, the temperature field of air is obtained from the density field of air using the ideal gas equation. The air temperature fields are obtained after normalizing the air density field and performing a calibration process by temperature values measured with a K-type thermocouple.

The velocity fields associated with the variation of the gradient of the refractive index of air were obtained by entering two consecutive images acquired at different times, t_1 and t_2, with a temporal separation Δt to the JPIV software [30,31]. JPIV uses the particle image velocimetry (PIV) technique and allows the velocity field calculation either between consecutive images or any other pair of images. JPIV has an interrogation window where the user can specify the window resolution and the conditions with the information will be extracted from the input images and then produce the desired results. These options include "multiple passes" pass 1,

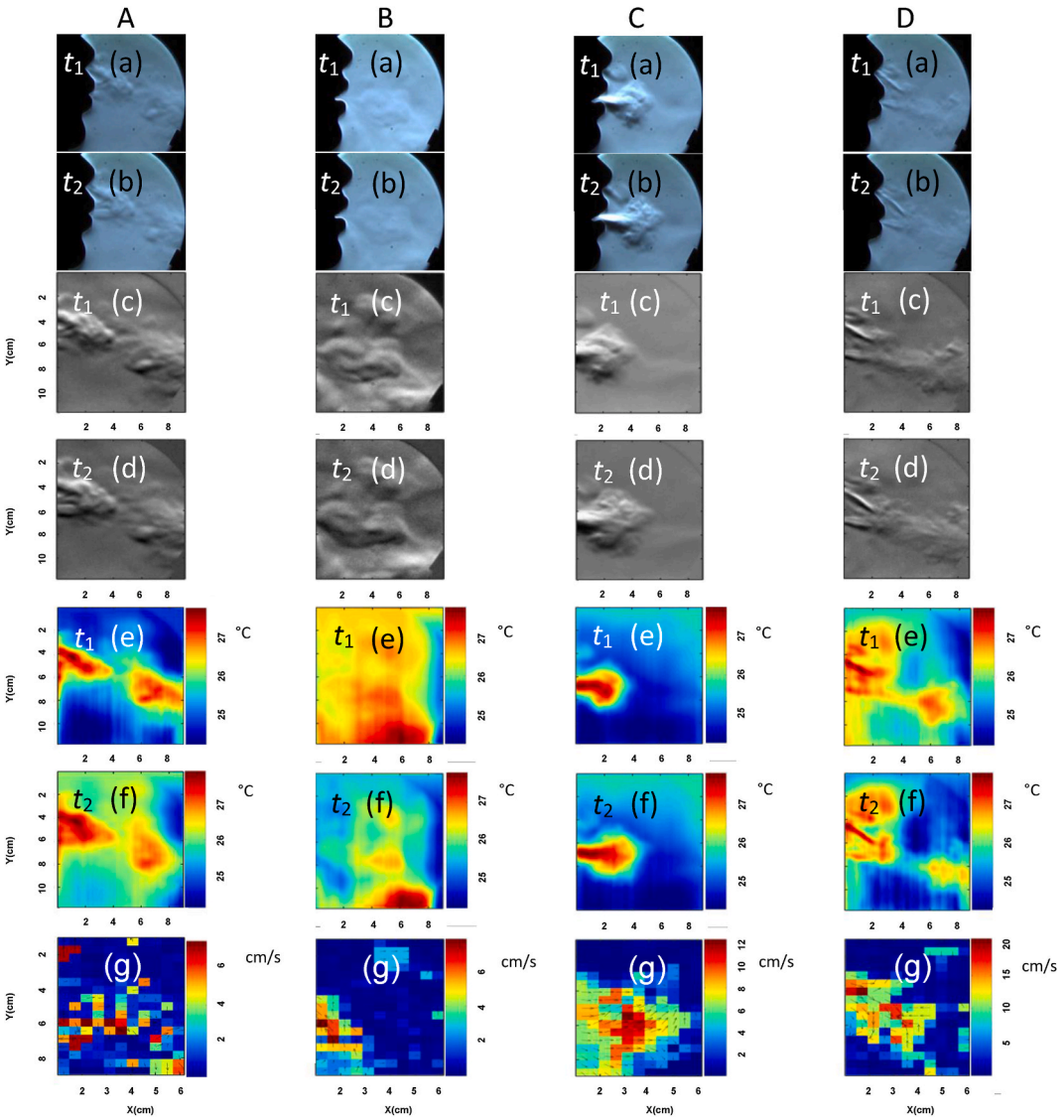

Fig. 4. (a), (b) Consecutive schlieren images, with a temporal difference of Δt = 0.022198 s between them, of all the output airflow tests considered in this research (A: talking; B: breathing; C: exhaling; and D: blowing) performed by a person (a 28 years old female subject) without using any respiratory mask. (c), (d) Refractive index gradient of the output airflow around the mouth of the subject, and (e), (f) temperature fields around the central zone of the output airflow calibrated with the temperatures shown in Table 1. (g) Velocity field around the central zone of the output airflow for all the tests performed. X and Y are the spatial coordinates in the horizontal and vertical directions, calibrated from the raw schlieren images.

pass 2, pass 3, interrogation window width (64, 32, 32), interrogation window height (64, 32, 32), search domain width (32, 8, 8), search domain height (32, 8, 8), horizontal vector spacing (32, 16, 12), and vertical vector spacing (32, 16, 12). The quality of the results is enhanced while the window size is reduced. In our particular case, JPIV uses the schlieren images that contain structures in movement associated with "pseudo-particles" that follow the airflow to obtain the displacement fields. We use 64 × 64 pixels windows applying the 3 × 3 median and 3 × 3 smoothing filters in obtaining the displacement vector in the first pass. Nevertheless, if a solution is not found, the software continues with the following "pass" using a 32 × 32 pixels window to enhance the quality of the airflow displacement vector. Finally, the JPIV software delivers the position vectors in the x and y directions and the displacement vectors in x and y in columns in a jcv format. Then, using the displacement vectors and the known time between the images, we calculate the velocity fields that we visualize using GNU Octave software.

4. Results and discussion

As was commented before, the main objective of this research is to visualize the airflow expulsed by a person while talking, breathing, exhaling, and blowing, wearing a disposable face mask inside a closed room. Although, we also studied each one of the airflow tests mentioned above performed by the same person but this time without using any respiratory mask but under the same conditions considered when was used a face mask. These additional tests were performed to establish a reference and show the changes in the density, temperature, and airflow velocity obtained by the optical technique used in the present work. In this way, from the simultaneous data analysis with and without a face mask, it was easy to calibrate both the values of the temperature and velocity of airflow. In Fig. 4 the images (a) and (b) show two consecutive raw schlieren images acquired during each one of airflow tests performed by a person without wearing a face mask. Certainly, Fig. 4 (a) and (b) show some important characteristics that describe the airflow expulsed by the person who completed the tests. Nevertheless, the gradient of the refractive index of air calculated from the raw schlieren images provides more contrast and more details about the characteristics of the turbulence of airflow exhaled by the subject performing the test, as shown in Fig. 4 (c) and 4 (d). To examine only the airflow details, the processed images from the raw images only show partially the subject performing the airflow tests. Fig. 4 (c) and 4 (d) show in gray scales the gradient of the refractive index of inhaled or exhaled air during each test obtained from the schlieren raw images shown in Fig. 4(a) and (b) acquired at two consecutive times t_1, and t_2 that differ by 0.022198 s. X and Y are the spatial coordinates in the horizontal and vertical directions calibrated from the raw schlieren images. Next, the temperature fields around the face masks were obtained from the gradient of the refractive index of air previously calculated. However, it was necessary to calibrate these temperature fields, comparing them with the temperatures shown in Table 1, measured with a K-type thermocouple coupled to a digital multimeter. Fig. 4(e) and (f) show the temperature fields corresponding to Fig. 4(c) and (d) obtained after processing both images in each case considered. The magnitude of the temperature in the central zone of the output airflow from the mask is indicated in the color scale (increasing from blue to red) on the right side of Fig. 4(c) and (d). The increment in the output airflow temperature regarding the environment temperature revealed by the processed schlieren images shows the presence of a subject perturbing the air, which now contains traces of CO_2 and a little more humidity than the fresh air entering the mask.

One of the characteristics of great interest in the airflow expulsed or inhaled during all the tests is the velocity field associated with the high variation of the gradient of the refractive index of air, calculated from the processing of the two images acquired at two consecutive times t_1 and t_2. By obtaining the velocity field, it is possible at least to estimate the distance traveled, for example, by the saliva droplets expelled by a person without or wearing a face mask during the airflow tests. As shown in Fig. 4(g) (at the central zone of airflow expulsed during the exhaling test), some particles reach speeds with values around 20 cm/s. However, there is a velocity distribution associated with the airflow presenting velocities ranging from 1 cm/s to 12 cm/s, as will be shown in Fig. 8(A)–8(D).

In the second test developed in this work, a person (the subject who performed all the tests) wearing a surgical three-ply face carried out all the airflow tests air, preferably in a horizontal direction close to the mirror of the experimental setup, as described in the schlieren images shown in Fig. 5(a) and (b). The air exhaled or inhaled through the face mask was performed perpendicularly to the light beam path in the experimental setup. Fig. 5(c) and (d) show the refractive index gradient of the output airflow obtained from the schlieren raw images processing shown in Fig. 5(a) and (b), which correspond to the two consecutive times t_1 and t_2 that differs again between them 0.022198 s. As shown in Fig. 5(a)–(b) is appreciable an output airflow from the mask, which is relatively warmer than the input fresh airflow through the face mask for the breathing, exhaling, and blowing tests, surely due to the size of the average filter

Table 1
The average temperature of the room where was performed the study of the airflow visualization without and using a face mask, and the average temperature of a zone close to the mouth (3 cm) of the person who completed all the tests, talking, breathing, exhaling, and blowing, measured with a K-type thermocouple coupled to a digital multimeter.

*Room Temperature = 24.20 °C

Type of mask	TEST			
	Talking	Breathing	Exhaling	Blowing
Without/Face Mask	27.62 °C	26.31 °C	27.8 °C	27.37 °C
Three-layer Surgical type	25.90 °C	26.29 °C	27.75 °C	25.28 °C
KN95	24.34 °C	24.78 °C	25.60 °C	25.68 °C
3M N95	24.07 °C	24.15 °C	24.91 °C	24.35 °C

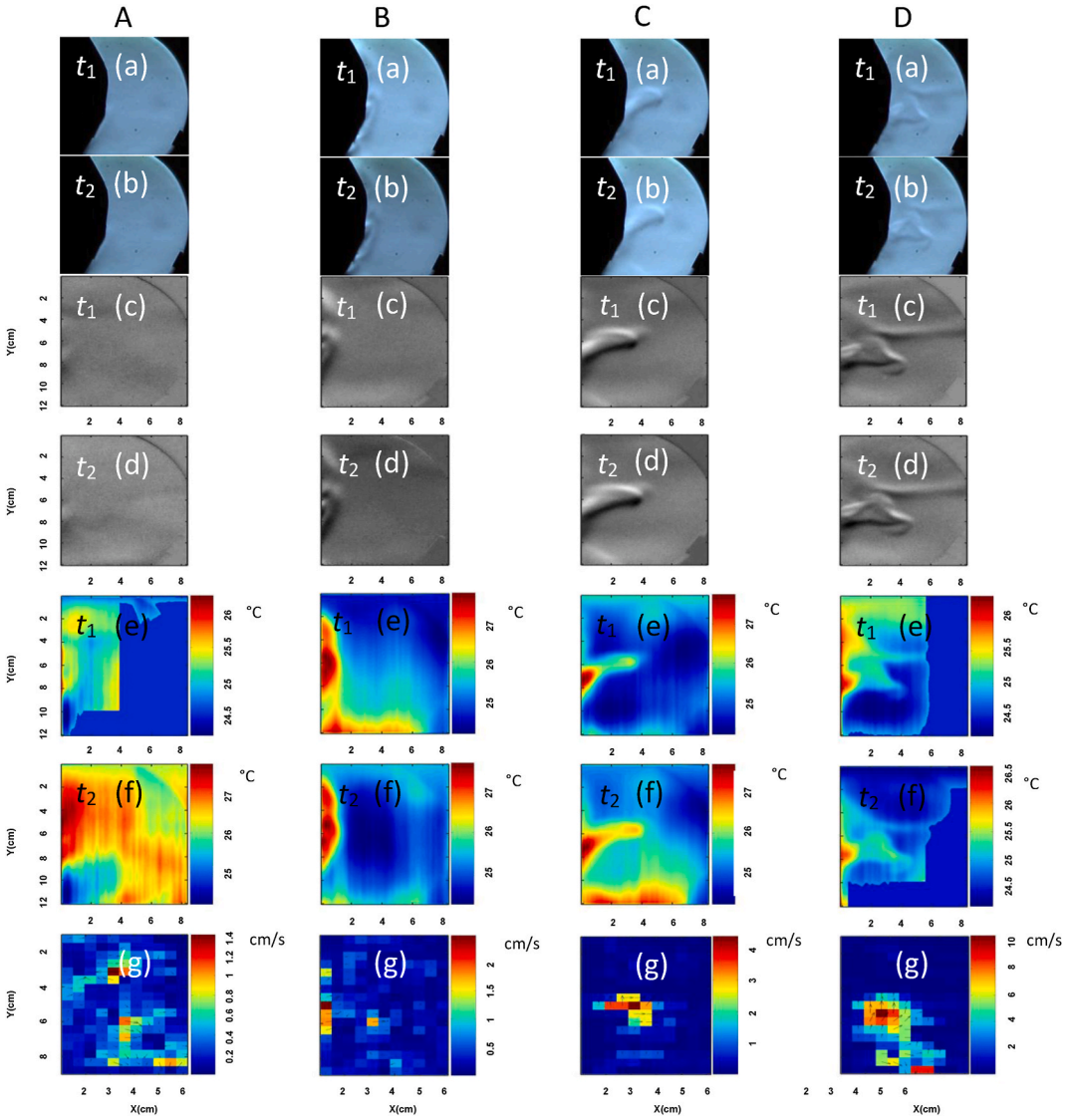

Fig. 5. (a), (b) Consecutive schlieren images of all the output airflow tests studied in this research (A: talking; B: breathing; C: exhaling; and D: blowing) performed by a person wearing a surgical three-ply face mask. (c), (d) Refractive index gradient of the output airflow around the mouth of the subject, and (e), (f) temperature fields around the central zone of the output airflow calibrated with the temperatures shown in Table 1. (g) Velocity field around the central zone of the output airflow.

pore provided by the three layers face mask composing, as shown in Fig. 2(k)-2(m). It is relevant to highlight that we can detect the output airflow from the mask thanks to this air is slightly warmer than the fresh air admitted through the mask. Also, the density of the output airflow is slightly higher than the air admitted through the mask since it contains traces of CO_2 and tiny amounts of water in the form of aerosol from saliva droplets that increase its humidity. On the other hand, as shown in Fig. 5(e) and (f) also can be appreciated noticeable variations of the outside temperature around the face mask, revealing the presence of a subject performing the airflow tests in the closed room where was performed this research. Again, was also obtained the velocities distribution of airflow inhaled or expulsed during all the tests. As shown in Fig. 5(g), the airflow expulsed during the blowing test reached speeds of up to 14 cm/s at a line crossing its central zone.

The third test of exhaled or inhaled airflow was performed wearing a KN95 face mask in similar conditions to the previous tests. Fig. 6(a) and (b) show two consecutive raw schlieren images acquired at times t_1 and t_2 as in the above tests, of the airflow exhaled or inhaled in a horizontal direction by the same person who performed all the tests. Fig. 6(c) and (d) show the refractive index gradient of air, obtained after to process the schlieren raw images shown in Fig. 6 (a) and 6 (b). As can be observed in Fig. 6(c)–(d) this time, there is almost an appreciable output airflow from the mask, which is relatively warmer than the input fresh airflow through the face mask. It can barely be possible to detect a small difference between the output and input airflows through the face mask thanks to the calculation of the gradient of the refractive index obtained from the schlieren images processing, as shown in Fig. 6(c)–(d) for the cases

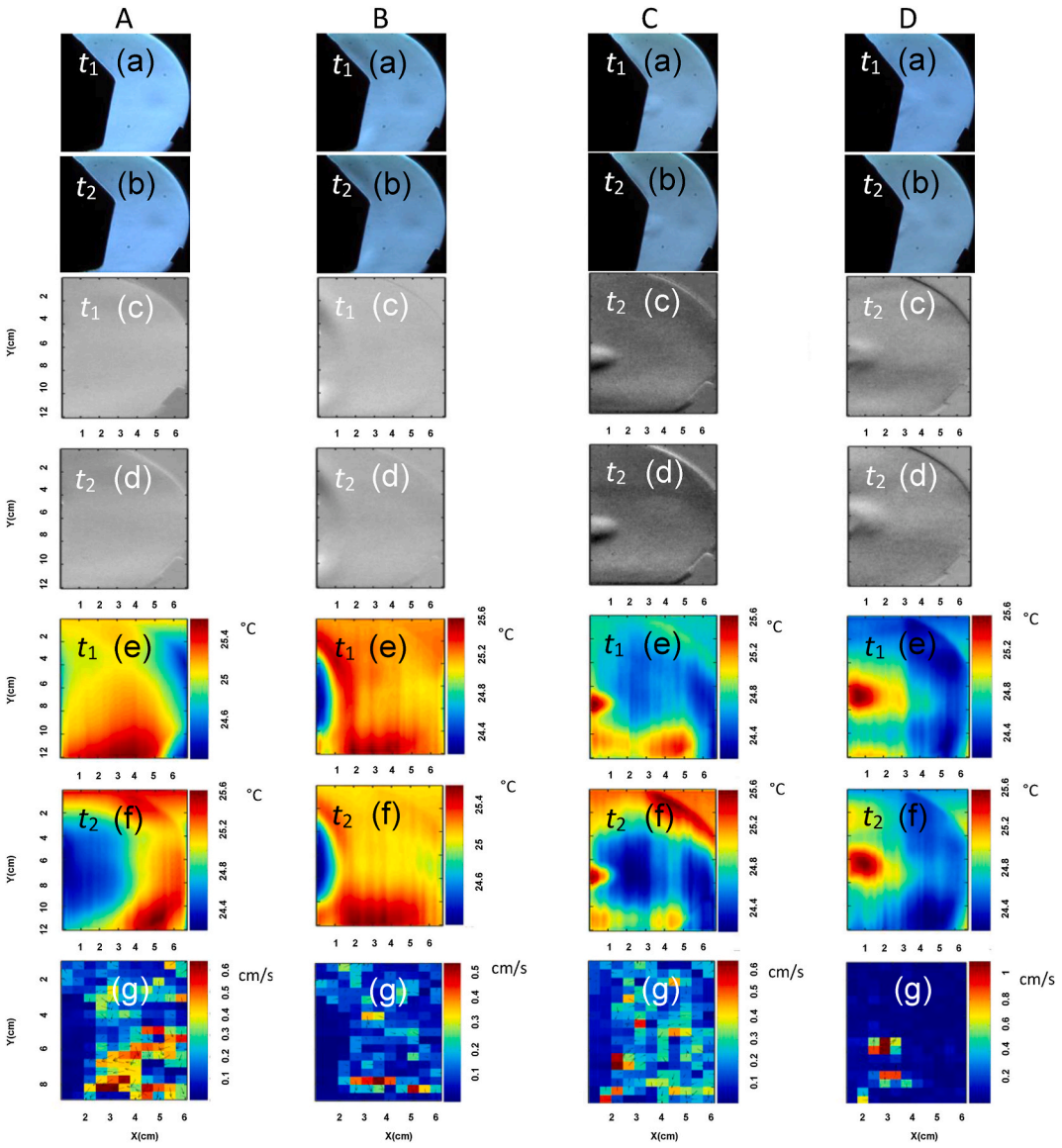

Fig. 6. (a), (b) Consecutive schlieren images of all the output airflow tests studied in this research (A: talking; B: breathing; C: exhaling; and D: blowing) performed by a person wearing a KN95-type face mask. (c), (d) Refractive index gradient of air around the mouth of the subject, and (f), (g) temperature fields around the central zone of airflow calibrated with the temperatures shown in Table 1. (g) Velocity field around the central zone of the output airflow.

of C: exhaling, and D: blowing. Regarding the temperature variations around the face mask, even though there seems to be a notable change in Fig. 6(e)–(f), but there is no, because the variation is barely 1 °C, as can be seen respectively, in the color scale on the right side of each Fig. The filtering capacity of the KN95-type face mask is very high since it inhibits the abrupt exit of a warmer output airflow with a density slightly higher than the fresh air admitted through the mask. As shown in Fig. 6(c)–(d), barely could be detected a small output airflow through the mask. In addition, the estimated airflow velocity expulsed by the subject wearing the mask is barely detectable and minor to 1 cm/s for all the tests developed, as shown in Fig. 6(g). Fig. 6(g) shows the velocities field obtained from the refractive index gradient of air calculated for the times t_1 and t_2.

Finally, the last test of inhaling or exhaling airflow was performed (in similar conditions to the previous tests) by a person wearing a 3MN95(Aura TC-84A-8590) face mask. Fig. 7(a)-(b) show two consecutive raw schlieren images taken at times t_1 and t_2 that differ from each other by a time of 0.11099 s of an exhaled or inhaled airflow in a horizontal direction. Fig. 7(c)–(d) show the refractive index gradient of air around the face mask. Again, to complete that calculation, the two consecutive schlieren raw images shown in Fig. 7(a)–(b) were processed to improve detection and reveal any possible output airflow with physical characteristics different from the fresh air admitted from the surroundings through the mask. The results obtained in this test allowed us to detect a little difference in the density, temperature, and probably the humidity between the output and input airflows through the face mask in practically all the cases.

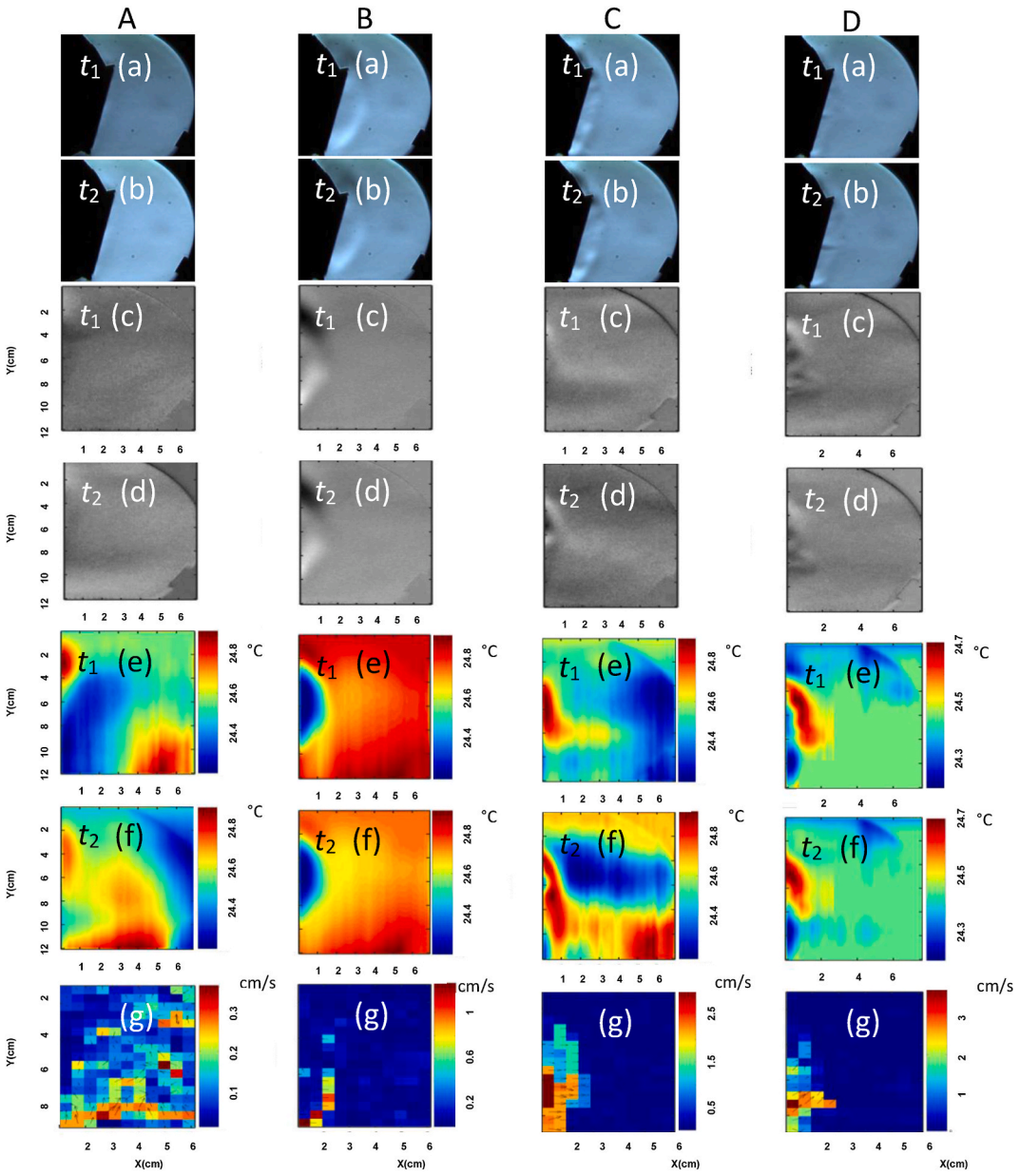

Fig. 7. (a), (b) Consecutive schlieren images of all the output airflow tests studied in this research (A: talking; B: breathing; C: exhaling; and D: blowing) performed by a person wearing a 3MN95 (Aura TC-84A-8590) face mask. (c), (d) Refractive index gradient of air around the mouth of the subject, and (e), (f) temperature fields around the central zone of output airflow calibrated with the temperatures shown in Table 1. (g) Velocity field around the central zone of output airflow.

However, for the "talking" test, there were no detected appreciable changes in the output and input airflows through the mask. The performance of the 3MN95(Aura TC-84A-8590) face mask was very similar to that observed for the test with the KN95 mask. Nevertheless, now there is a difference a little greater between the output and input airflows through the face mask than in the case of the KN95 face mask, as is revealed from the calculation of the refractive index gradient of air and the calculation of the temperature fields shown in Fig. 7(c)–(f). However, these variations on the refractive index gradient of air and its temperature around the 3MN95 face mask are certainly small regarding the results obtained for the KN95 face mask. The temperature variations in the case of the 3MN95 face mask are also lower than 1 °C. Even so, the maximum value of these variations is extended in a zone whose average length is around 6 cm, which is greater than in the case of the KN95 face mask, as can be observed and compared in Fig. 6(e)–(f) and Fig. 7(e)-(f). On the other hand, the magnitude of the average velocity of the airflow is slightly higher than in the case of the KN95 face mask test, except in the case of the "A: talking" test as can be shown in Fig. 6 (g) and 7 (g) and more clearly in Fig. 8(A). From the velocities fields shown in Fig. 6(g) and 7(g) obtained from the gradient of the refractive index of air, it is observed that now the maximum velocity

slightly exceeds 3 cm/s while in the test of KN95 mask not exceeds 1 cm/s. Is interesting to observe how the filtering capacity of the KN95 mask is a little minor to the efficiency of 3MN95 only in the "A: Talking" test. Since both masks fit well on the face, this fact has its origin in the different morphology and size of the polypropylene fibers of the middle layers in the 3MN95 mask whose appearance looks messier than the corresponding PP fibers the of the KN95 face mask, as can be observed in Fig. 2(a)-2(j).

To recapitulate the results of the velocity distribution in the output airflow through each one of the face masks used, we have included in Fig. 8(A)–8(D) the magnitude of the velocity as a function of the distance along the *x* coordinate for all the tests carried out. The *x* coordinate is along a direction perpendicular to the path of the light beam in the schlieren setup. It is defined in each case, finding first the maximum magnitude of the velocity in the central zone of the output airflow and moving then to the right at a constant height. As can be observed in Fig. 8(A)–8(D), it is easy to detect which one of the face masks used has the higher filtering capacity related to the inhibition of an abrupt exit of warmer airflow with a density slightly higher than the fresh air admitted through the mask and its propagation velocity in each test. The airflow expulsed from the KN95 mask is practically equal to the input airflow, and the few "pseudo-particles" expulsed that could be distinguished from the "pseudo-particles entering the face mask have a velocity approximately equal to zero. It is easy to observe in Fig. 8(A)–8(D) how the 3MN95 mask exhibits a difference in the density and temperature between the output and input airflows a little greater than the KN95 mask, except in the "A: talking" test. Although the airflow velocity expelled from the 3MN95 is low, such that its maximum value reached for the "D: blowing test" is around 3 cm/s as shown in Fig. 8(D). However, it is relevant to comment that the airflow velocity magnitude expelled from the 3MN95 face mask decreases quickly with the distance increasing. Fig. 8(A)–8(D) show how the velocity of particles expelled into the air from the 3MN95 face mask is practically zero for distances greater than 3 cm.

In summary, the present research shows interesting results about some physical parameters that characterize the airflow expulsed or inhaled by a person while "A: talking; B: breathing; C: exhaling; and D: blowing" wearing a disposable face mask inside a closed room. The Schlieren optical technique has allowed us to visualize the airflow through three disposable face masks during all the output airflow tests considered and performed by one person wearing one at a time. This research shows that two of the three tested face masks efficiently limit the output airflow, which presents a little difference in the density, temperature, and humidity regarding the input airflow through the face mask in practically all cases. However, one of them, the generic KN95-type face mask, presented the lowest abrupt output airflow in the field of view of the experimental setup used (in a horizontal direction and at a specific height from the floor), potentially offering a higher protection to people around a hypothetic subject performing a test like the reported in this research.

It is important to mention that the results obtained in this research have some limitations since the tests were performed by a single person performing a single type of speech, breathing, exhaling, and blowing. The reason for that is the impossibility of performing repeated tests that yield an enormous amount of information that must be processed. The processing of high-volume information demands a high computing infrastructure and people support to carry out the airflow tests. There is also a field of vision limited by the size of the mirror in the experimental setup that does not allow to capture air leakage above and below the face masks. Other limitation of the technique used is the low contrast of the particles tracing the airflow on the schlieren images obtained because of their low density. Although the schlieren technique is one of the most sensible to study low-density and low-speed airflows, sometimes the airflow characteristics limit the quantification of their properties. However, despite all these limitations, the aim of our work was satisfied since it was possible to show that the method used works in the visualization of airflows to which our experiment refers, and

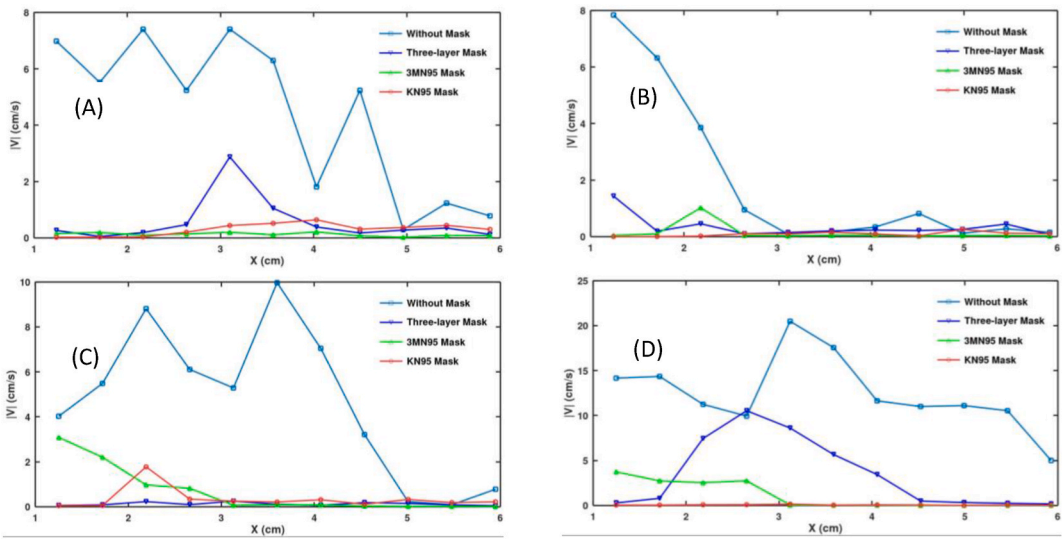

Fig. 8. Velocity distribution profile of output airflow for all the tests studied in this research (A: talking; B: breathing; C: exhaling; and D: blowing) along a horizontal line in the *x* direction at a specific height in its central zone. The "without face mask test" is denoted by (□), and the tests using face masks by (▽) surgical three-layer, (Δ) 3MN95 (Aura TC-84A-8590), and (○) KN95 type. The line was taken in each case, locating first the maximum magnitude of velocity in the central zone of the airflow and moving then to the right at a constant height.

this is the relevant point. The results found in this research contribute to understanding the airflow dynamics through a disposable face mask used by a person because were reported quantitative estimations of some of the physical parameters that characterize it.

5. Conclusions

We have presented an exhaustive visualization, including 112 images of the airflow expulsed by a person talking, breathing, exhaling, and blowing air while wearing a disposable face mask inside a closed room. The optical schlieren experimental arrangement used in the experimentation allowed us to obtain the magnitude of some of the more relevant physical parameters of the airflow through the face mask, such as the refractive index gradient, the temperature distribution in its surroundings, and the associated velocity field. The research was conducted using three face masks, one of the surgical types and two very similar to each other belonging to the N95 series with denominations KN95 and 3MN95 (Aura TC-84A-8590), respectively. The results show that the surgical mask is the one that allows the most abrupt output airflow in the field of view of the experimental setup. The other two face masks, the KN95 and 3MN95, have a similar performance since both efficiently limit the output airflow, which presents a little difference in the density, temperature, and humidity regarding the input airflow through the face mask. However, there were found some differences between them. The KN95 face mask had the best performance since it presented the lowest output airflow (with different physical properties to the input airflow) to its surroundings for all the tests except for the "talking" test. Therefore, we can conclude that the KN95-type face mask could provide more safety by restricting the flow of potential pathogens from the mouth or nose from one person to another. The results presented in this work show the great potential of the Schlieren techniques to determine the airflow behavior around a face mask, which can help to reduce and prevent the risk of spreading infectious airborne particles.

CRediT authorship contribution statement

Cornelio Alvarez-Herrera: Visualization, Validation, Software, Resources, Methodology, Investigation, Formal analysis, Data curation, Conceptualization. **Jose G. Murillo-Ramirez:** Writing – review & editing, Writing – original draft, Visualization, Validation, Supervision, Resources, Project administration, Methodology, Investigation, Formal analysis, Data curation, Conceptualization.

Declaration of competing interest

The authors declare that they have no known competing financial interests or personal relationships that could have appeared to influence the work reported in this paper.

Acknowledgments

This work was published with the support of Instituto de Innovación y Competitividad de la Secretaría de Innovación y Desarrollo Económico del Estado de Chihuahua, México. The authors would like to thank Itzel Cárdenas Aceves, for helping to perform all the airflow tests without and wearing the face masks used in this study. Also, they thank Karla Campos Venegas, from the Laboratorio Nacional de Nanotecnología (NaNoTeCh) at Centro de Investigación en Materiales Avanzados S. C., for obtaining the SEM micrographs of face masks. José G. Murillo-Ramírez thanks CONAHCYT México for the Complementary Support received for Sabbatical Stays linked to the Consolidation of Research Groups (2022).

Appendix A. Supplementary data

Supplementary data to this article can be found online at https://doi.org/10.1016/j.heliyon.2024.e33384.

References

[1] W. Peters, G. Pasvol, 5-Infecciones transmitidas por el aire, Atlas de medicina tropical y parasitología, Elsevier, Spain, 2008, pp. 273–289, https://doi.org/10.1016/B978-84-8086-283-7.50005-1.
[2] R.P. Wenzel, A.A. Fowler 3rd, Clinical practice. Acute bronchitis, N. Engl. J. Med. 355 (20) (2006) 2125–2130, https://doi.org/10.1056/NEJMcp061493.
[3] E.R. Wald, N. Guerra, C. Byers, Upper respiratory tract infections in young children: duration of and frequency of complications, Pediatrics 87 (2) (1991) 129–133, https://doi.org/10.1542/peds.87.2.129.
[4] R. Tellier, Y. Li, B.J. Cowling, J.W. Tang, Recognition of aerosol transmission of infectious agents: a commentary, BMC Infect. Dis. 19 (1) (2019) 1–9, https://doi.org/10.1186/s12879-019-3707-y.
[5] O.M. Morakinyo, M.I. Mokgobu, M.S. Mukhola, R.P. Hunter, Health outcomes of exposure to biological and chemical components of inhalable and respirable particulate matter, Int. J. Environ. Res. Publ. Health 13 (6) (2016) 1–22, https://doi.org/10.3390/ijerph13060592, 592.
[6] F.J. Kelly, J.C. Fussell, Size, source and chemical composition as determinants of toxicity attributable to ambient particulate matter, Atmos. Environ. 60 (2012) 504–526, https://doi.org/10.1016/j.atmosenv.2012.06.039.
[7] World Health Organization, Dietary and Inhalation Exposure to Nano- and Microplastic Particles and Potential Implications for Human Health, Licence: CC BY-NC-SA 3.0 IGO, Geneva, 2022. https://www.who.int/publications/i/item/9789240054608.
[8] J.B. Fink, S. Ehrmann, J. Li, P. Dailey, P. McKiernan, C. Darquenne, A.R. Martin, B. Rothen-Rutishauser, P.J. Kuehl, S. Häussermann, R. MacLoughlin, G. C. Smaldone, B. Muellinger, T.E. Corcoran, R. Dhand, Reducing aerosol-related risk of transmission in the era of COVID-19: an interim guidance endorsed by the International Society of Aerosols in Medicine, J. Aerosol Med. Pulm. Drug Deliv. 33 (6) (2020) 300–304, https://doi.org/10.1089/jamp.2020.1615.

[9] C.B. Beggs, The airborne transmission of infection in hospital buildings: fact or fiction? Indoor Built Environ. 12 (1–2) (2003) 9–18, https://doi.org/10.1177/1420326O3032201.
[10] H.T. Bausum, S.A. Schaub, K.F. Kenyon, M.J. Small, Comparison of coliphage and bacterial aerosols at a wastewater spray irrigation site, Appl. Environ. Microbiol. 43 (1) (1982) 28–38, https://doi.org/10.1128/aem.43.1.28-38.1982.
[11] J.W. Tang, Y. Li, I. Eames, P.K.S. Chan, G.L. Ridgway, Factors involved in the aerosol transmission of infection and control of ventilation in healthcare premises, J. Hosp. Infect. 64 (2) (2006) 100–114, https://doi.org/10.1016/j.jhin.2006.05.022.
[12] R.B. Patel, S.D. Skaria, M.M. Mansour, G.C. Smaldone, Control de la fuente respiratoria mediante el uso de una mascarilla quirúrgica: un estudio in vitro, J. Occup. Environ. Hyg. 18 (sup.1) (2021) S25–S34, https://doi.org/10.1080/15459624.2021.1877068.
[13] K.B. Rogers, An investigation into the efficiency of disposable face masks, J. Clin. Pathol. 33 (11) (1980) 1086–1091, https://doi.org/10.1136/jcp.33.11.1086.
[14] J.W. Tang, T.J. Liebner, B.A. Craven, G.S. Settles, A schlieren optical study of the human cough with and without wearing masks for aerosol infection control, J. R. Soc. Interface 6 (6) (2009) S727–S736, https://doi.org/10.1098/rsif.2009.0295.focus.
[15] J. Pan, C. Harb, W. Leng, L.C. Marr, Inward and outward effectiveness of cloth masks, a surgical mask, and a face shield, Aerosol, Sci. Technol. 55 (6) (2021) 718–733, https://doi.org/10.1080/02786826.2021.1890687.
[16] W.H. Seto, D. Tsang, R.W.H. Yung, T.Y. Ching, T.K. Ng, M. Ho, L.M. Ho, J.S.M. Peiris, Advisors of Expert SARS group of Hospital Authority, Effectiveness of precautions against droplets and contact in prevention of nosocomial transmission of severe acute respiratory syndrome (SARS), Lancet 361 (9368) (2003) 1519–1520, https://doi.org/10.1016/S0140-6736(03)13168-6.
[17] D.K. Chu, E.A. Akl, S. Duda, K. Solo, S. Yaacoub, H.J. Schünemann, COVID-19 Systematic Urgent Review Group Effort (SURGE) study authors, Physical distancing, face masks, and eye protection to prevent person-to-person transmission of SARS-CoV-2 and COVID-19: a systematic review and meta-analysis, Lancet 395 (10242) (2020) 1973–1987, https://doi.org/10.2139/ssrn.3578764.
[18] X. Xie, Y. Li, H. Sun, L. Liu, Exhaled droplets due to talking and coughing, J. R. Soc. Interface 6 (6) (2009) S703–S714, https://doi.org/10.1098/rsif.2009.0388.focus.
[19] G.R. Johnson, L. Morawska, Z.D. Ristovski, M. Hargreaves, K. Mengersen, C.Y.H. Chao, M.P. Wan, Y. Li, X. Xie, D. Katoshevski, S. Corbett, Modality of human expired aerosol size distributions, J. Aerosol Sci. 42 (12) (2011) 839–851, https://doi.org/10.1016/j.jaerosci.2011.07.009.
[20] China Food and Drug Administration, Standardization Administration of China (SAC) Pharmaceutical Industry Standard of the People's Republic of China, Standard YY/T 0969-2013 Single-use medical face mask,.https://www.chinesestandard.net/PDF.aspx/YYT0969-2013.
[21] Centers for Disease Control and Prevention, The national Institute for occupational safety and health (NIOSH), NIOSH guide to the selection and use of particulate respirators, 96-101, http://www.cdc.gov/niosh/docs/96-101/, 1996.
[22] Standardization Administration of China (SAC), China Standard GB 2626-2019 Respiratory Protection-Non-Powered Air-Purifying Particle Respirator Original, 2020. https://www.cps.bureauveritas.com/newsroom/china-mandatory-standard-gb-2626-2019-respiratory-protection-non-powered-air-purifying.
[23] European Committee for standardization CEN/TC 79, European Standard EN 149:2001+A1:2009, Respiratory protective devices - filtering half masks to protect against particles - requirements. Testing, Marking "(FFP) Mask, 2009. https://www.cencenelec.eu/news-and-events/news/2020/pressrelease/2020-03-20-cen-and-cenelec-make-european-standards-available-to-help-prevent-the-covid-19-contagion/.
[24] K. O'Dowd, K.M. Nair, P. Forouzandeh, S. Mathew, J. Grant, R. Moran, J. Bartlett, J. Bird, S.C. Pillai, Face masks and respirators in the fight against the COVID-19 pandemic: a review of current materials, advances and future perspectives, Materials 13 (15) (2020) 1–27, https://doi.org/10.3390/ma13153363, 3363.
[25] C. Alvarez-Herrera, J.G. Murillo-Ramírez, I. Pérez-Reyes, D. Moreno-Hernández, Proper orthogonal decomposition applied to laminar thermal convection in a vertical two plate channel, J. Opt. 17 (6) (2015) 065602, https://doi.org/10.1088/2040-8978/17/6/065602.
[26] B. Sendyka, W. Mitianiec, M. Noga, Study of combustion process with jet-ignition of propane-air mixtures, Bull. Pol. Acad. Sci. Tech. Sci. 63 (2) (2015) 533–543, https://doi.org/10.1515/bpasts-2015-0061.
[27] C. Alvarez-Herrera, J.L. Herrera-Aguilar, D. Moreno-Hernández, A.V. Contreras-García, J.G. Murillo-Ramírez, 3D flame reconstruction and error calculation from a schlieren projection, J. Eur. Opt. Soc. Rapid. Publ. 16 (21) (2020) 1–13, https://doi.org/10.1186/s41476-020-00141-8.
[28] D. Derrick, N. Kabaliuk, L. Longworth, P. Pishyar-Dehkordi, M. Jermyet, Speech air flow with and without face masks, Sci. Rep. 12 (2022) 837, https://doi.org/10.1038/s41598-021-04745-z.
[29] W. Merzkirch, Flow Visualization, second ed., Academic Press, Inc, Orlando, United States of America, 1987.
[30] M. Raffel, C. Willert, J. Kompenhans, Particle Image Velocimetry: A Practical Guide, second ed., Springer-Verlag, Berlin Heidelberg, 2007.
[31] J. Westerweel, Digital Particle Image Velocimetry: Theory and Application, Delft University Press, 1993.